FOI
SWEDISH DEFENCE
RESEARCH AGENCY

FOI-R--0277--SE
December 2001
ISSN 1650-1942
Scientific report

Anna Häggström

Connecting Thrust and Torque with the Wake Tip Vortex Geometry – Application to Wind Turbines and Propellers

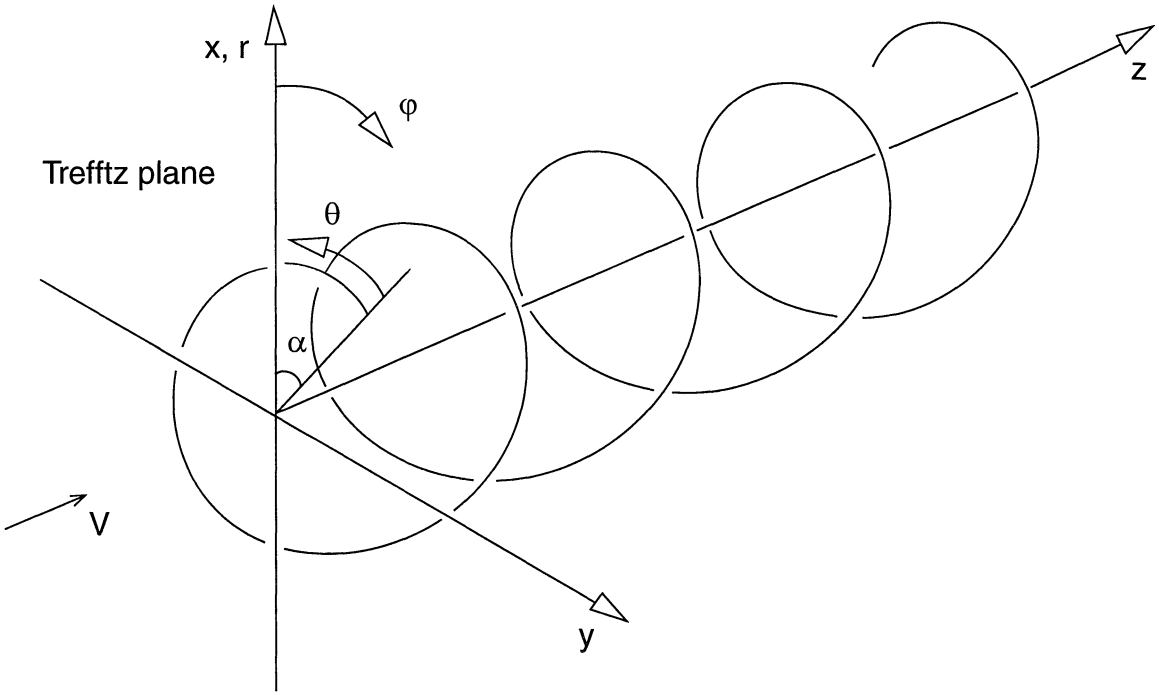

Aeronautics Division, FFA
SE-172 90 Stockholm

SWEDISH DEFENCE RESEARCH AGENCY
Aeronautics Division, FFA
SE-172 90 Stockholm

FOI-R--0277--SE
December 2001
ISSN 1650-1942
Scientific report

Anna Häggström

Connecting Thrust and Torque with the Wake Tip Vortex Geometry – Application to Wind Turbines and Propellers

Issuing organization
FOI – Swedish Defence Research Agency
Aeronautics Division, FFA
SE-172 90 Stockholm

Report number, ISRN
FOI-R--0277--SE

Report type
Scientific report

Research area code
9. Civil applications

Month year
December 2001

Project no.
E870318

Customers code
5. Contracted Research

Sub area code
91 Civil Applications

Author
Anna Häggström

Project manager
Björn Montgomerie

Approved by
Sven-Erik Thor

Sponsoring agency
Swedish National Energy Administration

Scientifically and technically responsible
Björn Montgomerie

Report title
Connecting Thrust and Torque with the Wake Tip Vortex Geometry – Application to Wind Turbines and Propellers

Abstract
Wind turbines and propellers have historically been analysed using either blade element momentum theory or vortex methods. This Master of Science thesis deals with the latter type.

In present free wake methods, the vortices trailing off the blades are assumed to be governed only by the Biot-Savart potential flow induction law, forming a helical surface sheet. In reality, partly due to viscosity, however, the vorticity is concentrated into tip vortices, one per blade tip, and into root vorticity of a more indistinct character. A look at some basic aspects of flow mechanics was seen as necessary to explain the discrepancy between present theory and reality.

The result of this work is a method to calculate radius and pitch of the concentrated tip vortex spirals, from given values of the thrust and torque coefficients C_T and C_Q and a given strength of the maximum circulation around the blade(s). To achieve this, the inverse problem must be solved. I.e., from known tip vortex spiral parameters the corresponding C_T and C_Q were first calculated and saved in a database. This database is henceforth used together with an interpolation routine, which makes inversion possible. The computer code for the inversion is also part of the thesis.

Keywords
wind power, turbine, aerodynamics, vortex, wake, performance

Further bibliographic information
Thesis for Masters degree in engineering

Language English

ISSN 1650-1942

Pages 47 p.

Price acc. to pricelist

Security classification open

Utgivare	Rapportnummer, ISRN	Klassificering
Totalförsvarets Forskningsinstitut - FOI	FOI-R--0277--SE	Vetenskaplig rapport
Flygteknik, FFA	**Forskningsområde**	
172 90 Stockholm	9. Övriga civila tillämpningar	
	Månad, år	**Projektnummer**
	December 2001	E870318
	Verksamhetsgren	
	5. Uppdragsfinansierad verksamhet	
	Delområde	
	91 Övriga civila tillämpningar	

Författare	Projektledare
Anna Häggström	Björn Montgomerie
	Godkänd av
	Sven-Erik Thor
	Uppdragsgivare/kundbeteckning
	Energimyndigheten
	Tekniskt och/eller vetenskapligt ansvarig
	Björn Montgomerie

Rapportens titel (i översättning)

Samband mellan axialkraft, axialmoment och spetsvirvelgeometri, med tillämpning för vindturbiner och propellrar

Sammanfattning

Vindturbiner och propellrar har historiskt sett analyserats med antingen bladelementteori eller virveltrådsmetoder. Detta examensarbete behandlar det senare området.

I tidigare virveltrådsmetoder har man antagit att virveltrådarna som lämnar bladet ges sin form av Biot-Savarts induktionslag enbart och bildar en skruvformad s.k. diskontinuitetsyta. Delvis på grund av viskositet koncentreras emellertid cirkulationen till virveltrådar, en tråd per bladspets, och till en mera diffus rotcirkulation.

Resultatet av arbetet är en metod att beräkna radie och stigning på spiralen som bildas av en spetsvirveltråd, utifrån givna värden på axialkraft- och axialmomentkoefficienterna C_T och C_Q och given maximal cirkulation runt bladet (bladen). Men först måste C_T och C_Q beräknas från antagen spiralgeometri, dvs för en matris av många kombinationer av radie och stigning. Härvid användes Biot-Savarts lag. Resultaten samlades i en databas. För att uppnå syftet måste sedan det inversa problemet lösas genom att använda en interpolationsrutin som bearbetar databasen. Interpolationskoden finns tillgänglig bland övrig kod från arbetet.

Nyckelord

vindkraft, turbin, aerodynamik, virvel, virvlar, vak, prestanda

Övriga bibliografiska uppgifter	Språk Engelska
Examensarbete för civilingenjörsexamen	
ISSN 1650-1942	**Antal sidor:** 47 s.
Distribution enligt missiv	**Pris: Enligt prislista** **Sekretess öppen**

Contents

Notation

Primed variables have a corresponding non-dimensional variable, where the latter is the only one used in the text.

Roman

$\bar{a} = \frac{\bar{v}}{V}$	Non-dimensional induced velocity
$a_x,\ a_y,\ a_z, a_\varphi$	x-, y-, z- respective φ-component of $\bar{a}$
$A_T = \pi R_T^2$	Turbine or propeller area
b	Number of blades
$\bar{C}$	Point in the Trefftz plane (z=0)
C_T	Thrust coefficient
C_Q	Torque coefficient
$d = \frac{d'}{R_T}$	Non-dimensional pitch (of tip vortex spiral)
$d_{root} = \frac{d_{root}'}{R_T}$	Non-dimensional pitch of root vortex spiral
$d\bar{S}$	Element on a vortex spiral
f	Function, integrand in Biot-Savart's law
$f(b,d,R)$	Function, defined in Section 5.6
$L = \frac{L'}{R_T}$	Non-dimensional length
L	Lift force
m	Mass
$\dot{m}$	Mass flow
p	Pressure
Q	Torque
$r = \frac{r'}{R_T}$	Non-dimensional cylinder coordinate
$\bar{r}_S$	Vector from a vortex element to an arbitrary point in the Trefftz plane (z=0)
$R = \frac{R_W}{R_T}$	Non-dimensional wake radius
$R_{core} = \frac{R_{core}'}{R_T}$	Non-dimensional core radius
R_{root}	Non-dimensional radius of root vortex spiral
R_T	Turbine or propeller radius
R_W	Wake radius
$\bar{S}$	Point on the vortex spiral
T	Thrust
$\bar{v}$	Induced velocity
V	Free stream wind velocity
$x = \frac{x'}{R_T}$	Non-dimensional Cartesian coordinate

$y = \frac{y'}{R_T}$	Non-dimensional Cartesian coordinate
$z = \frac{z'}{R_T}$	Non-dimensional Cartesian coordinate; parallel to the free stream wind.

Greek

α	Starting angle of a trailing vortex
$\gamma = \frac{\Gamma}{R_T V}$	Non-dimensional circulation
Γ	Circulation
θ	Independent spiral coordinate
ρ	Air density
φ	Cylinder coordinate

1 Introduction

Blade element momentum theory and vortex sheet theory are theories that are widely used when analysing wind turbines and propellers. However, there are many situations where they are not valid but still used. This may be the case, for example, in rapid changes of wind direction or wind velocity, in wind turbine shutoffs, for calculating initial takeoff thrust of an airplane propeller or for modelling flows that are time variable or oblique to the disk. Therefore, there is a need for a new method, which is reliable in such situations as well. The *concentrated vortex theory* is assumed to be such a theory, if applied as a time variant problem.

This work deals with a part problem in the concentrated vortex theory, that is to find *radius* and *pitch* of the concentrated tip vortex spiral, from given values of thrust and torque coefficients and a given strength of the maximum circulation around the blade(s). The theory is valid for wind turbines and propellers alike and the word *airscrew* will be used for both of these.

Many complicating situations may arise during operation of a wind turbine. This thesis is limited to the symmetrical case, thus excluding any guidance for dealing with e.g. yaw or wind shear. Within this work, airscrews with one to three blades are studied.

2 Background

To understand the new method and the need of such, some background information might be needed. This section describes different theories used for load calculations on wind turbines and propellers.

2.1 Actuator disk theory

The simplest model for understanding the aerodynamics of a propeller or turbine is the actuator disk theory, where a disk with the same radius substitutes the rotor. The actuator disk is quite an inexact approximation, since all effects are averaged over the disk area. No consideration is made of the rotor geometry, which may play an important role for the performance. However, the basic momentum equations that this theory builds on are the same as in the vortex methods and deserve a review.

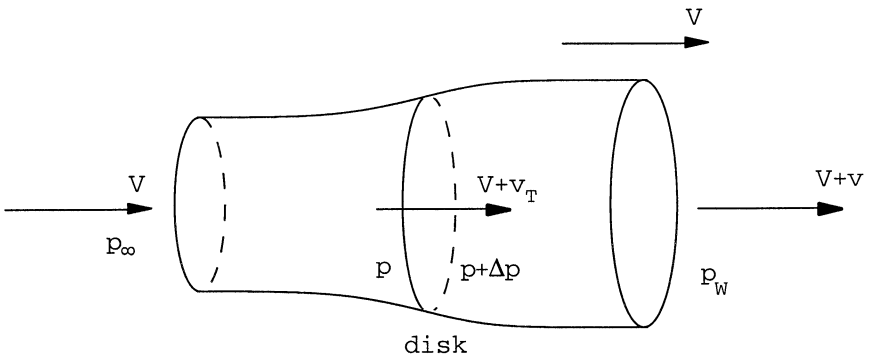

Figure 2.1
Actuator disk

Assumptions are made that the slipstream of the rotor is clearly defined and the air moving outside the slipstream is practically undisturbed. Consider a cylindrical control volume, which encloses the rotor and the slipstream as shown in Figure 2.1. Upstream of the rotor, the wind velocity is undisturbed and is denoted by V. As the air approaches the rotor, the wind velocity decreases (turbine) or increases (propeller) and far downstream it has decreased or increased to $V + v$, where v is negative for a turbine and positive for a propeller. The airflow is continuous and hence there is no sudden change of the velocity at the rotor. However, there is a discontinuous change in the pressure at the disk, which corresponds to the rotor thrust. That is,

$$T = \pi R_T^2 \Delta p \,. \tag{2.1}$$

The total force in the axial direction on the control surface consists of both the rotor thrust and the pressure forces acting on the ends of the control volume. By the *momentum theorem*, the total force equals the rate of change of momentum. With the notations defined Figure 2.1, this means

$$T + \pi R_W^2 (p_\infty - p_W) = \rho \pi R_W^2 (V + v) v \,. \tag{2.2}$$

From this equation, the thrust can be solved as

$$T = \rho \pi R_W^2 (V + v) v + \pi R_W^2 (p_W - p_\infty) \,. \tag{2.3}$$

Bernoulli's equation gives that

$$p + \tfrac{1}{2} \rho V^2 = \text{constant} \,. \tag{2.4}$$

If Bernoulli's equation is applied at points upstream of the rotor, we get

$$p_\infty + \frac{1}{2} \rho V^2 = p_T + \frac{1}{2} \rho (V + v_T)^2 \tag{2.5}$$

and for points downstream we get

$$p_T + \Delta p + \frac{1}{2}\rho(V + v_T)^2 = p_W + \frac{1}{2}\rho(V + v)^2 . \tag{2.6}$$

Solving for Δp gives

$$\Delta p = p_W - p_\infty + \rho\left(V + \tfrac{1}{2}v\right)v . \tag{2.7}$$

Since the airflow is continuous, we have

$$\rho(V + v_T)R_T^2 = \rho(V + v)R_W^2 \tag{2.8}$$

and by this, (2.3) can be rewritten

$$\frac{T}{\pi R_T^2} = \Delta p = \rho(V + v_T)v + \frac{V + v_T}{V + v}(p_W - p_\infty) . \tag{2.9}$$

Equating (2.7) and (2.9) gives

$$\rho v\left(v_T - \tfrac{1}{2}v\right) = (p_W - p_\infty)\frac{(v - v_T)}{V + v} . \tag{2.10}$$

If the value of the wake pressure is evaluated far from the rotor, it is reasonable to assume that the wake pressure equals the ambient pressure, i.e. $p_W = p_\infty$. Then (2.10) gives

$$v_T = \tfrac{1}{2}v , \tag{2.11}$$

i.e. the induced velocity at the rotor is half the induced velocity in the far wake and hence, from (2.9) the torque can be calculated as

$$T = 2\rho\pi R_T^2(V + v_T)v_T . \tag{2.12}$$

Similarly, the torque can be calculated as the rate of change of moment of momentum. Under the same assumptions as above, the torque becomes

$$Q = 2\rho\pi R_T^2(V + v_T)v_T r . \tag{2.13}$$

As can be seen in the formulas, this method requires that either the thrust (or torque) or the induced velocity is known.

2.2 Blade element momentum theory

One step up in complexity and accuracy is the blade element momentum theory. The blade is subdivided into a number of blade elements, whose forces are determined using known airfoil characteristics. A summation of thrust contributions from all blades, from all elements on the same radius, is then matched with the momentum loss or gain of the wake flow. From (2.2) the induced velocity and hence the flow velocity decrease or increase can be calculated.

This method is reliable in many situations and has low requirements on computer speed. However, as mentioned in the introduction, there are several situations where it is not valid.

2.3 Vorticity

For a wing to experience a lift force, the average pressure must be higher on the lower side than on the upper. Equation (2.4), Bernoulli's theorem, illustrates how pressure increases when velocity decreases. Hence the air velocity must be higher over the upper surface of the wing than the lower. To achieve this a circulation around the wing can be superposed to the free stream wind, as illustrated in Figure 2.2.

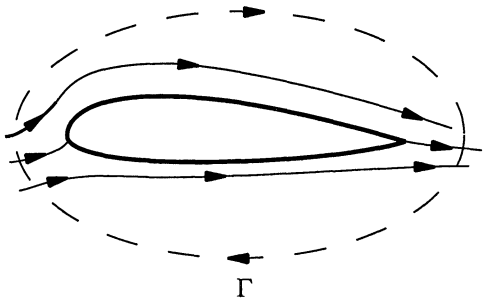

Figure 2.2
Air flow around a wing.

According to the *Kutta-Joukowski theorem*, the lift force per unit span can be calculated as

$$L = \rho V \Gamma , \tag{2.14}$$

where V is the undisturbed wind velocity and Γ is the circulation.

Helmholtz's theorem gives that vorticity cannot terminate in the interior of a fluid. The circulation around a blade element continues as free vortex lines trailing from the edges of the blade element, as is shown in Fig. 2.3.

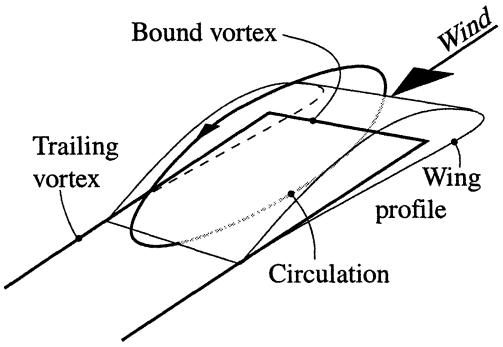

Figure 2.3
Vorticity trailing from a blade element.

If the vorticity varies along the blade, the difference in circulation is trailed off, forming a vortex sheet behind the wing. This is illustrated in Figure 2.4 where $\Delta\Gamma$ is the descretized sheet representation.

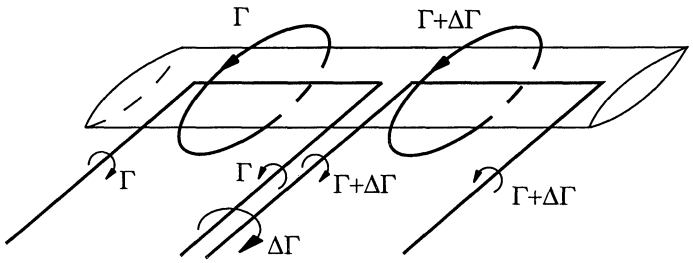

Figure 2.4
Trailing vorticity, forming a vortex sheet.

2.4 Vortex sheet theory

Vortex theory depends on the fact that it is possible to separate the wake from the airscrew and still be able to calculate thrust and torque. That means, with no prior knowledge of the characteristics of the airscrew that generated the vortex spiral, both thrust and torque can be calculated from the wake characteristics alone.

The so-called free wake model contains the idea that the trailing vorticity described in Section 2.3 can be modelled to leave the wing representation (which frequently is only a straight line) like a silkworm fibre. The blade is subdivided into a number of blade elements and one such vortex trails from its corresponding blade element. The trailing vorticity is modelled in the computer as piecewise straight lines with circulation, each such segment being used to induce velocities on all other segments. The induction can be calculated using potential flow theory, notably the Biot-Savart law, which will be described in Section 3:2. After summation over all segments, a total induced velocity is obtained for each segment. Multiplication by the chosen time step in the simulation gives the translation of the whole vortex system. The new vortex system is also used for calculation of the induced velocities on the blade itself. One induced velocity will be evaluated at each blade element whereby the local flow is known at the blade element.

After completion of one such cycle, the aerodynamic load on the element is calculated. The calculated load is then converted to a new value of bound vorticity and a new piece of vortex is trailed from the wing representation, etc. Thus, the vorticity is allowed to develop in response to whatever happens on the blades.

Plots of vorticity trailed from a wind turbine or propeller blade in a simulation, according to the description above, shows how an apparent screw surface is slightly deformed as it travels downstream. However, smoke injection in the stream tube in real turbine flows shows that the vorticity does not travel as a screw surface but rather as a concentrated vortex trailing off the tip of each blade and as a more diffuse root vorticity. The fact that the vorticity is concentrated is also, in humid air, clearly visible for example behind an airplane, where the vorticity is concentrated into a single vortex trailing off each wing.
This behavior is caused by viscosity, which is not modeled within the vortex sheet theory based on potential flow. This leads to the idea of the concentrated vortex theory.

2.5 Concentrated vortex theory

It is desirable to model the real flow, as it is observed to behave, for mainly two reasons. There is partly the hope that a more nature-like model will give results that are more exact. In addition, the concentrated tip vortex represents an enormous reduction of calculational effort. With a concentrated tip vortex model in place of the "classical" free wake model, even aeroelastic code, containing such an aerodynamic model, will be within manageable bounds to allow parametric studies.

Before the concentrated vortex theory is usable, one question needs an answer. That is, to what radius should the concentrating trailing vorticity travel? Since the potential flow method gives partly misleading guidance in this respect, some other method of finding radius and pitch of the trailing tip vortex spiral must be found. The matching of thrust and torque with the trailing tip vorticity geometry is the idea, which is developed for this purpose in this report. When the appropriate tip vortex radius and pitch are found, in each time step of the simulation, the instantaneous thrust and torque are available since they are known from blade element calculation. Consolidations of this method can later be accomplished, as results from measurements become available.

The root vortex, trailing from an airscrew, can be modelled either as a straight line vortex along the wake centre axis, with circulation in the opposite direction to that of the tip vortices and whose

strength is equal to the added strength of all the tip vortices, or in the same way as the tip vortices. In the latter case, the radius depends on the shape of the blade and the pitch is calculated, to a good approximation, from the characteristics of the tip vortex. This work deals mainly with the case of the root vortex modeled as a straight line. However, some comments and examples on different root vortex models are made in Sect. 7.

3 Mathematical formulation of the problem

3.1 Non-dimensioning

The solution of the problem should encompass all sizes of airscrews. The technique includes elimination of physical dimensions. In order to get a dimensionless problem the thrust and the torque are normalized; resulting in the dimensionless variables called C_T and C_Q. Wake radius, pitch, circulation and induced velocity are also normalized and turned dimensionless. To get the normalization consistent, all variables are normalized against the corresponding rotor parameters and the free stream wind velocity. Then the same equations hold for the normalized and the non-normalized variables. For the definitions of the non-dimensional variables, see Table of Notations on page 7. Angles are not normalized.

The thrust and torque coefficients are given as

$$C_T = \frac{T}{\frac{1}{2}\rho V^2 A_T} \tag{3.1}$$

and

$$C_Q = \frac{Q}{\frac{1}{2}\rho V^2 R_T A_T}. \tag{3.2}$$

3.2 Biot-Savart's law

To calculate the velocity induced by a vortex line an analogy in the theory of electromagnetism, called the Biot-Savart law, can be used. Applied to our problem the *Biot-Savart law* becomes

$$\bar{a} = \frac{\gamma}{4\pi}\int \frac{\bar{r}_S \times d\bar{S}}{r_S^3}, \tag{3.3}$$

where $\bar{r}_S$ is the vector from the point of evaluation to a point on the vortex and $d\bar{S}$ is along the vortex line. Inside the wake, a turns out positive for a propeller and negative for a turbine.

For a straight vortex line of length L, the induced velocity becomes

$$\bar{a} = \frac{\gamma}{2\pi r_\perp}\frac{L}{\sqrt{L^2 + r_\perp^2}}\bar{e}_\varphi \quad \rightarrow \quad \frac{\gamma}{2\pi r_\perp}\bar{e}_\varphi, \quad when\ L >> r_\perp, \tag{3.4}$$

where $r_\perp$ is the shortest distance between the vortex line and the evaluation point and $\bar{e}_\varphi$ is a unit vector.

3.3 The core

The integrand in the Biot-Savart law is singular in points at the vortex line. This would correspond to infinite velocities, but of course, this cannot be the real case. Therefore, a core is introduced, such that the induced velocity is decreasing inside the core and is zero in points at the vortex line. The technique used in the approximation of the induced velocity is to replace r accordingly

$$\frac{1}{r} \approx \frac{r}{r^2 + R_{core}^2}, \tag{3.5}$$

where r is the distance between the vortex line and the point of evaluation and R_{core} is the core radius. This is illustrated in Figure 3.1.

According to Bhagwat and Leishman (2001), the physical size of the core radius is about 1% of the rotor radius. This is the core radius size used in the calculations. Bhagwat and Leishman have also

drawn the conclusion that the induced velocities do not depend strongly on the core velocity distribution.

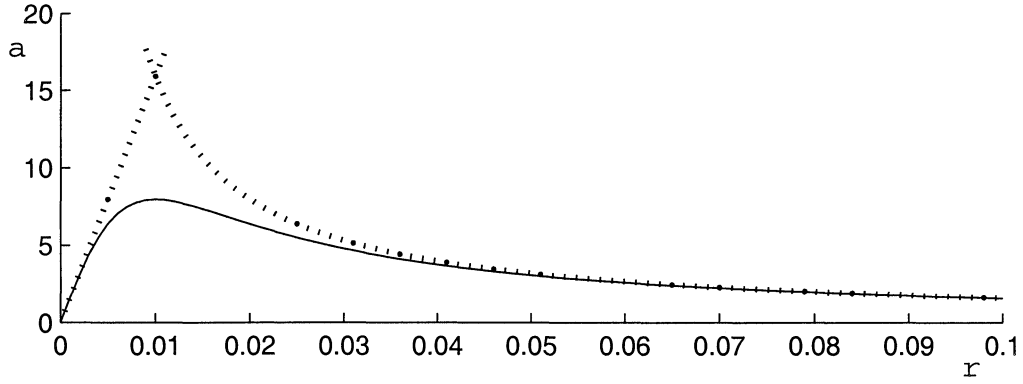

Figure 3.1

The smooth full curve represents induced velocity of an infinitely long straight vortex line placed in r = 0. In this example is $R_{core} = 0.01$ and $\gamma = 1$. The dotted lines correspond to the induced velocity without a core, i.e. $a = \frac{\gamma}{2\pi r}$, *outside the core and the straight line* $a = \frac{\gamma}{2\pi R_{core}^2} r$ *inside the core.*

3.4 Coordinate systems

Since there is a cylindrical symmetry, it is natural to use cylindrical coordinates for purposes of explanation. The positive z-axis is chosen in the free stream wind direction, with $z = 0$ in Trefftz plane, i.e. the xy-plane where the flows are evaluated. The vortex lines form spirals, whose coordinates are uniquely determined from the pitch (d), radius of spiral (R) and azimuth angle ($\varphi = \alpha - \theta$) where θ is the independent spiral coordinate and α is the starting point for the actual vortex line.

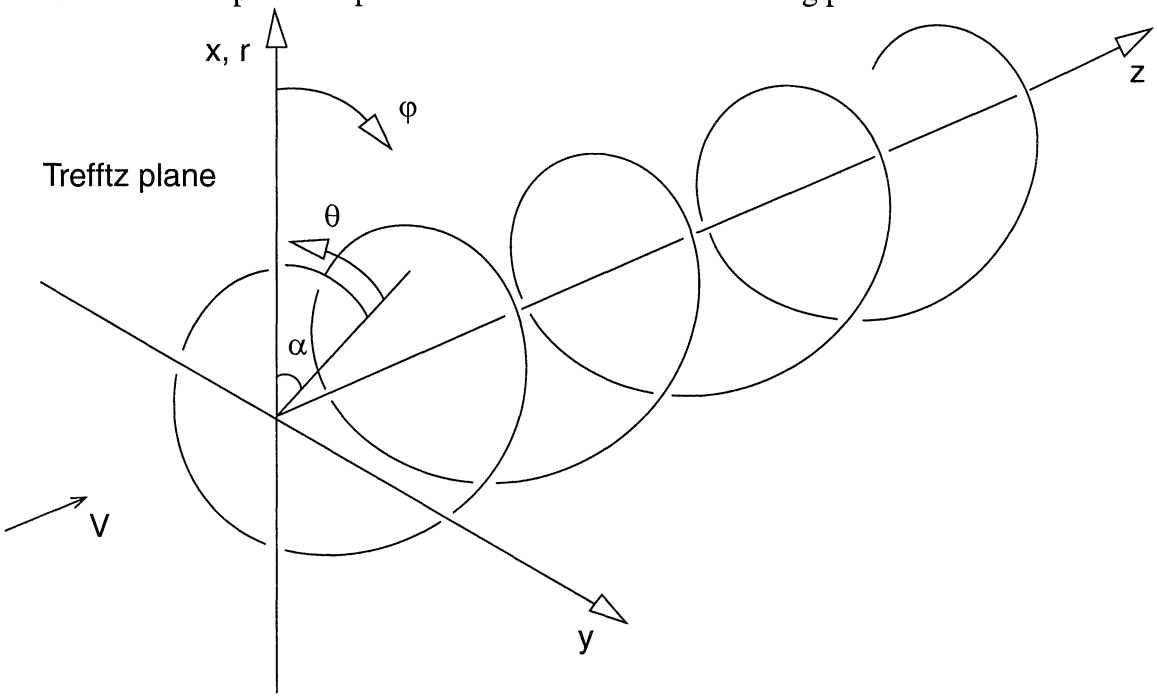

Figure 3.2

Definition of the coordinate system.

It is also useful to have available the Cartesian coordinates. A point S on the vortex has Cartesian coordinates

$$\bar{S}(\theta)=\left(R\cos(\alpha-\theta),\quad R\sin(\alpha-\theta),\quad \frac{d}{2\pi}\theta \right) \tag{3.6}$$

and a point C in the Trefftz plane has coordinates

$$\bar{C}(r,\varphi)=(r\cos(\varphi),\quad r\sin(\varphi),\quad 0). \tag{3.7}$$

The vector $\bar{r}_S$ from C to S becomes, in Cartesian coordinates,

$$\bar{r}_S(r,\varphi,\theta)=\bar{S}-\bar{C}=\left(R\cos(\alpha-\theta)-r\cos(\varphi),\quad R\sin(\alpha-\theta)-r\sin(\varphi),\quad \frac{d}{2\pi}\theta \right) \tag{3.8}$$

and an element $d\bar{S}$ along the vortex spiral has the equation

$$d\bar{S}(\theta)=\left(R\sin(\alpha-\theta),\quad -R\cos(\alpha-\theta),\quad \frac{d}{2\pi} \right)d\theta. \tag{3.9}$$

3.5 Application of Biot-Savart's law in the different directions

Inserting the above relations in (3.3), Biot-Savart's law, gives the following expressions for the velocities induced by b vortices, corresponding to b blades. The last terms in the expressions for a_x and a_y correspond to the root vorticity, which is modelled as a straight line.

$$a_x=\frac{\gamma d}{(2\pi)^2}\sum_{i=1}^{b}\int_0^{\infty}\frac{R\sin(\alpha_i-\theta)-r\sin(\varphi)+R\cos(\alpha_i-\theta)\theta}{\left(R^2+r^2-2rR\cos(\alpha_i-\theta-\varphi)+\left(\frac{d}{2\pi}\theta\right)^2 \right)^{\frac{3}{2}}}d\theta+b\frac{\gamma}{2\pi r}\cos(\varphi), \tag{3.10}$$

$$a_y=\frac{\gamma d}{(2\pi)^2}\sum_{i=1}^{b}\int_0^{\infty}\frac{-R\cos(\alpha_i-\theta)+r\cos(\varphi)+R\sin(\alpha_i-\theta)\theta}{\left(R^2+r^2-2rR\cos(\alpha_i-\theta-\varphi)+\left(\frac{d}{2\pi}\theta\right)^2 \right)^{\frac{3}{2}}}d\theta-b\frac{\gamma}{2\pi r}\sin(\varphi), \tag{3.11}$$

$$a_z=\frac{\gamma}{2\pi}\sum_{i=1}^{b}\int_0^{\infty}\frac{-R^2+rR\cos(\alpha_i-\theta-\varphi)}{\left(R^2+r^2-2rR\cos(\alpha_i-\theta-\varphi)+\left(\frac{d}{2\pi}\theta\right)^2 \right)^{\frac{3}{2}}}d\theta. \tag{3.12}$$

Due to the symmetry in $\theta = 0$, integration is only made from zero to infinity. The total induced velocity is obtained by multiplication by 2.

Since both the summation (finite) and the integral ($\sim 1/\theta^2$ or $1/\theta^3$ for large θ) are convergent, an interchange of the integral and the summation is allowed.

The induced velocity in the φ-direction is given by

$$a_\varphi=-a_x\sin(\varphi)+a_y\cos(\varphi). \tag{3.13}$$

Also, the following relations are true and will be used

$$a_x=-a_\varphi\sin(\varphi) \tag{3.14}$$

$$a_y=a_\varphi\cos(\varphi) \tag{3.15}$$

3.6 Calculation of C_T and C_Q

The momentum theory is described in Section 2.1. With the assumption that the pressure in the final wake equals the ambient pressure, i.e. $p_W = p_\infty$, (2.3) gives that the contribution to thrust can be calculated as

$$dT = -v_z d\dot{m} = -v_z \rho(V + v_z) dA . \tag{3.16}$$

The minus sign is there in order to make T positive for wind turbines and negative for propellers, which is the definition used in this work. The expression is evaluated in the so-called Trefftz plane (see Figure 3.2), which is a plane perpendicular to the wake and placed infinitely far behind the airscrew.

Similarly, the torque contribution can be calculated from the corresponding moment of momentum theory as

$$dQ = -v_\varphi r d\dot{m} = -v_\varphi \rho(V + v_z) r dA . \tag{3.17}$$

This gives, in normalized variables,

$$dC_T = -\frac{2}{\pi} a_z (1 + a_z) r dr d\varphi \tag{3.18}$$

and

$$dC_Q = -\frac{2}{\pi} a_\varphi (1 + a_z) r^2 dr d\varphi . \tag{3.19}$$

Summation gives

$$C_T = -\frac{2}{\pi} \int_0^\infty \int_0^{2\pi} a_z d\varphi r dr - \frac{2}{\pi} \int_0^\infty \int_0^{2\pi} a_z^2 d\varphi r dr = C_{T_1} + C_{T_2} \tag{3.20}$$

and

$$C_Q = -\frac{2}{\pi} \int_0^\infty \int_0^{2\pi} a_\varphi d\varphi r^2 dr - \frac{2}{\pi} \int_0^\infty \int_0^{2\pi} a_z a_\varphi d\varphi r^2 dr = C_{Q_1} + C_{Q_2} . \tag{3.21}$$

Each integral in (3.20) and (3.21) will be treated separately in the calculations. The right hand sides of the expressions define notations that will be used further down the text.

It is notable that the induced velocities in the formulas above denote the *total* induced velocity, that is the velocity induced by both the tip vortices and the root vorticity.

The integrands in C_{TI} and C_{QI} are proportional to $1/r$ for large radii and hence, these integrals seem not to converge. However, due to counteraction between the tip vortices and the root vorticity and due to the spiral form of the vortex lines, these integrals cancel outside the wake. This will be investigated in more detail in Section 5.3.

4 Method

The main task was to solve the problem numerically, by making a large database for C_T and C_Q as functions of the spiral parameters R, d and γ and of the number of blades on the airscrew. An interpolation routine, which also was constructed, makes it possible to solve the inverse problem, which is the more interesting problem. It means that R and d will be functions of the given parameters C_T, C_Q and γ.

During the work, some useful explicit relations emerged after inspection of some numerical results. In order to limit the calculation time and to get a more exact result, these relations were analysed and used in the calculations. Some of these relations are proved. For them, both the numerical and the analytical solutions are presented in this report. Other relations are only motivated by the exact agreement with the numerical results. The latter type can be thought of as "curve fits".

All dependences are not completely solved with the method mentioned and hence a numerical solution is still needed. However, thanks to the explicit relations found only a small part of the problem needs be solved numerically.

All numerical calculations are made using Fortran programming. Matlab was used to make graphs.

5 Explicit results

5.1 Dependence of γ

From (3.3), the Biot-Savart law, it follows directly that the induced velocity is proportional to γ. Hence

$$C_{T_1} \sim \gamma, \tag{5.1}$$

$$C_{Q_1} \sim \gamma, \tag{5.2}$$

$$C_{T_2} \sim \gamma^2 \tag{5.3}$$

and

$$C_{Q_2} \sim \gamma^2. \tag{5.4}$$

5.2 Relation found for C_T/C_Q

From numerical calculations it can be deduced that if the root vortex is modelled as a straight line,

$$\frac{C_T}{C_Q} = \frac{2\pi}{d}. \tag{5.5}$$

It is noteworthy that the quotient depends on neither R nor γ. This relation is true independently of the number of blades of the airscrew.

This relation is also true for the components of C_T and C_Q term by term, i.e.

$$\frac{C_{T1}}{C_{Q1}} = \frac{C_{T2}}{C_{Q2}} = \frac{2\pi}{d}. \tag{5.6}$$

As will be shown in Section 5.3, it is exact for C_{T1}/C_{Q1}. For C_{T2}/C_{Q2}, it is very close to the numerical results. That the term-by-term relation (5.6) is consistent with (5.5) is proven by

$$\frac{C_T}{C_Q} = \frac{C_{T_1} + C_{T_2}}{C_{Q_1} + C_{Q_2}} = \frac{\frac{2\pi}{d} C_{Q_1} + \frac{2\pi}{d} C_{Q_2}}{C_{Q_1} + C_{Q_2}} = \frac{\frac{2\pi}{d}\left(C_{Q_1} + C_{Q_2}\right)}{C_{Q_1} + C_{Q_2}} = \frac{2\pi}{d}. \tag{5.7}$$

The same relation is also true if the integration in the r-direction is omitted. That is, the ratio of the mean values of a_z and a_φ or a_z^2 and $a_z a_\varphi$ on a fixed radius equals $2\pi r/d$.

Summarising these statements in a mathematical form gives

$$\frac{C_T}{C_Q} = \frac{\int_0^\infty \int_0^{2\pi} a_z \, d\varphi \, r dr}{\int_0^\infty \int_0^{2\pi} a_\varphi \, d\varphi \, r^2 dr} = \frac{\int_0^\infty \int_0^{2\pi} a_z^2 \, d\varphi \, r dr}{\int_0^\infty \int_0^{2\pi} a_z a_\varphi \, d\varphi \, r^2 dr} = \frac{\int_0^{2\pi} a_z^2 \, d\varphi}{\int_0^{2\pi} a_z a_\varphi \, d\varphi \, r} = \frac{\int_0^{2\pi} a_z \, d\varphi}{\int_0^{2\pi} a_\varphi \, d\varphi \, r} = \frac{2\pi}{d}, \tag{5.8}$$

which are true for all R, d, γ and b. These relations were all found out by numerical calculations.

5.3 The integrals of a_z and a_φ

5.3.1 Calculating the lift on an airfoil

The integrals of a_z and a_φ are quite similar to those of a well-known, analytically solvable problem. Consider the wake of an aeroplane wing, where the two tip vortices are parallel and the induced velocity is directed downwards inside the wake (Figure 5.1).

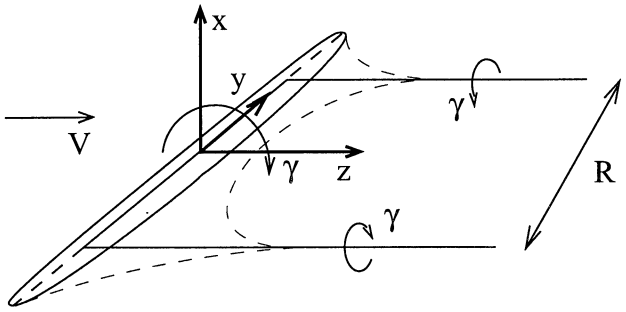

Figure 5.1
Airfoil wake

To calculate the lift force, the momentum flux is integrated in a similar way as in our problem. If R is the distance between the vortices,

$$L = \rho V \frac{\Gamma}{2\pi} \int_{-\infty}^{\infty}\int_{-\infty}^{\infty} \left(\frac{\frac{R}{2}+y}{\left(\frac{R}{2}+y\right)^2 + x^2} + \frac{\frac{R}{2}-y}{\left(\frac{R}{2}-y\right)^2 + x^2} \right) dx dy . \tag{5.9}$$

Integration in the vertical (x-) direction results in a step function (see for example Schlichting and Truckenbrodt (1960)), which equals $\rho V \Gamma$ inside the wake and zero outside. This step function is easily integrated in the horizontal (y-) direction, giving

$$L = \rho V \Gamma R . \tag{5.10}$$

5.3.2 Numerical solution of the integrals of a_z and a_φ

Having the result of the airfoil case in mind, we have an idea how to transfer the knowledge to our problem. The x-direction in the airfoil case corresponds to the φ-direction in the airscrew case. Numerical integration of $\int_0^{2\pi} a_z d\varphi$ and $\int_0^{2\pi} a_\varphi d\varphi$, with a fine division in the φ-direction, gives, as expected, functions that are very close to zero outside the wake (Figure 5.2 and Figure 5.3). Hence, the conclusion is drawn that they, in fact, are exactly zero there and that the deviation arises from numerical errors.

Numerical calculations also show that the integrals of $a_z d\varphi$ and $a_\varphi d\varphi$ are directly proportional to the number of blades.

Thus, from several numerical calculations it can be deduced that

$$\int_0^{2\pi} a_z d\varphi = \begin{cases} -2\pi b \dfrac{\gamma}{d}, & 0 < r < R \\ 0, & R < r \end{cases} \tag{5.11}$$

and

$$\int_0^{2\pi} a_\varphi d\varphi = \begin{cases} -b \dfrac{\gamma}{r}, & 0 < r < R \\ 0, & R < r \end{cases} . \tag{5.12}$$

Relation (5.11) and (5.12) have also been proven analytically, which will be shown in Section 5.3.3. The analytical solutions were found rather late in the work, which is why the numerical solutions are also included in the report.

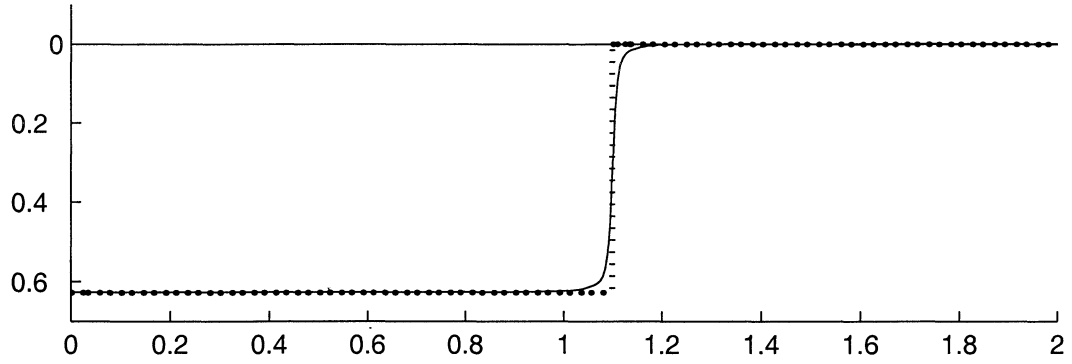

Figure 5.2
The result of a numerical integration of $a_z d\varphi$ (solid line), compared to the function (5.11) (dotted). ($b = 1$, $R = 1.1$, $d = 5$, $\gamma = 0.5$, $R_{core} = 0.01$.)

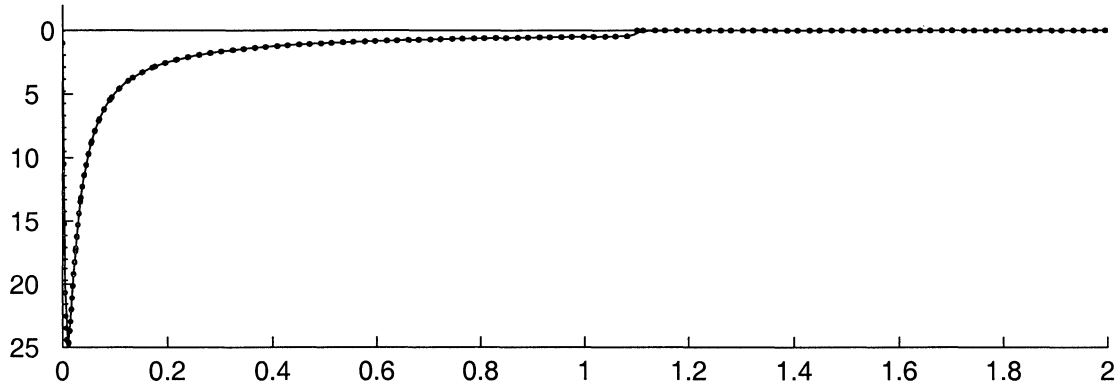

Figure 5.3
The result of a numerical integration of $a_\varphi d\varphi$ (solid line), compared to the function (5.12) (dotted). ($b = 1$, $R = 1.1$, $d = 5$, $\gamma = 0.5$, $R_{core} = 0.01$.)

The integration in the r-direction is easily done, giving

$$C_{T_1} = -\frac{2}{\pi}\int_0^\infty\int_0^{2\pi} a_z d\varphi\, r dr = 2b\frac{\gamma}{d}R^2 \tag{5.13}$$

and

$$C_{Q1} = -\frac{2}{\pi}\int_0^\infty\int_0^{2\pi} a_\varphi d\varphi\, r^2 dr = b\frac{\gamma}{\pi}R^2\,. \tag{5.14}$$

Inserting the results in (3.20) and (3.21) gives

$$C_T = 2b\frac{\gamma}{d}R^2 + C_{T_2} \tag{5.15}$$

and

$$C_Q = b\frac{\gamma}{\pi}R^2 + C_{Q_2}\,. \tag{5.16}$$

5.3.3 Analytical solution of the integral of a_z

Comparing with (3.12), which shows the definition a_z, we see that the integral of a_z is given by

$$\int_0^{2\pi} a_z\,d\varphi = \frac{\gamma}{2\pi}\sum_{i=1}^{b}\int_0^{2\pi}\int_0^{\infty}\frac{-R^2+rR\cos(\alpha_i-\theta-\varphi)}{\left(R^2+r^2-2rR\cos(\alpha_i-\theta-\varphi)+\left(\frac{d}{2\pi}\theta\right)^2\right)^{\frac{3}{2}}}d\theta\,d\varphi. \tag{5.17}$$

Hence, the integral that needs to be solved is

$$\int_0^{2\pi}\int_0^{\infty}\frac{-R^2+rR\cos(\alpha_i-\theta-\varphi)}{\left(R^2+r^2-2rR\cos(\alpha_i-\theta-\varphi)+\left(\frac{d}{2\pi}\theta\right)^2\right)^{\frac{3}{2}}}d\theta\,d\varphi. \tag{5.18}$$

$\cos(\alpha_i-\theta-\varphi)$ can here be substituted by $\cos(\varphi)$, since for every θ the integrand is 2π-periodical in φ. Then

$$(5.18)=\int_0^{\infty}d\theta\int_0^{2\pi}\frac{-R^2+rR\cos(\varphi)}{\left(R^2+r^2-2rR\cos(\varphi)+\left(\frac{d}{2\pi}\theta\right)^2\right)^{\frac{3}{2}}}d\varphi= \tag{5.19}$$

$$=\int_0^{2\pi}d\varphi\left(-R^2+rR\cos(\varphi)\right)\int_0^{\infty}\frac{d\theta}{\sqrt{\left(R^2+r^2-2rR\cos(\varphi)+\left(\frac{d}{2\pi}\theta\right)^2\right)^3}}. \tag{5.20}$$

Let

$$\theta=\frac{2\pi}{d}\sqrt{R^2+r^2-2rR\cos(\varphi)}\cdot\nu. \tag{5.21}$$

Then

$$d\theta=\frac{2\pi}{d}\sqrt{R^2+r^2-2rR\cos(\varphi)}\cdot d\nu \tag{5.22}$$

and

$$\left(\frac{d}{2\pi}\theta\right)^2=\left(R^2+r^2-2rR\cos(\varphi)\right)\cdot\nu^2. \tag{5.23}$$

Inserting this substitution in (5.20) gives

$$(5.20)=\int_0^{2\pi}d\varphi\left(-R^2+rR\cos(\varphi)\right)\frac{2\pi}{d}\frac{1}{\left(R^2+r^2-2rR\cos(\varphi)\right)}\int_0^{\infty}\frac{d\nu}{\sqrt{1+\nu^2}^3}= \tag{5.24}$$

$$=\int_0^{2\pi}d\varphi\left(-R^2+rR\cos(\varphi)\right)\frac{2\pi}{d}\frac{1}{\left(R^2+r^2-2rR\cos(\varphi)\right)}\cdot 1= \tag{5.25}$$

$$=\frac{2\pi}{d}\int_0^{2\pi}\frac{-R^2+rR\cos(\varphi)}{R^2+r^2-2rR\cos(\varphi)}d\varphi= \tag{5.26}$$

$$= \frac{2\pi}{d}\left[-R^2 \frac{2\pi}{\left|R^2 - r^2\right|} + rR \frac{1}{-2rR}\left(2\pi - \left(R^2 + r^2\right)\frac{2\pi}{\left|R^2 - r^2\right|} \right) \right]_0^{2\pi} = \tag{5.27}$$

$$= \frac{2\pi}{d}\left(-\pi - 2\pi\left(\frac{R^2}{\left|R^2 - r^2\right|} - \frac{1}{2}\frac{R^2 + r^2}{\left|R^2 - r^2\right|} \right) \right) = \tag{5.28}$$

$$= \frac{2\pi}{d}\left(-\pi - \pi\frac{R^2 - r^2}{\left|R^2 - r^2\right|} \right) = \begin{cases} -\dfrac{(2\pi)^2}{d} & \text{if } r < R \\ 0 & \text{if } R < r \end{cases} \tag{5.29}$$

Since the integral in (5.18) does not depend on the starting angle α_i, the summation in (5.18) may be substituted by multiplication with b. Inserting the result (5.29) in (5.18) gives

$$\int_0^{2\pi} a_z \, d\varphi = \begin{cases} -2\pi b\dfrac{\gamma}{d}, & 0 < r < R \\ 0, & R < r \end{cases}, \tag{5.30}$$

which is exactly (5.11).

5.3.4 Analytical solution of the integral of a_φ

For solving the integral of a_φ, a formula from the theory of electromagnetism is useful; namely *Ampère's circuital law*. (See for example Cheng (1989).) Translated to our variables it becomes

$$\oint \bar{a} \cdot d\bar{l} = \gamma_{tot} \,, \tag{5.31}$$

where the integral is taken along any closed path and γ_{tot} is the total non-dimensional circulation enclosed by the curve. The integration curve is chosen as a circle with radius r, that is

$$d\bar{l} = r d\varphi \, \bar{e}_\varphi \,. \tag{5.32}$$

For $r > R$, the total enclosed circulation is $\gamma_{tip} + \gamma_{root} = b\gamma - b\gamma = 0$ and hence

$$\oint \bar{a} \cdot d\bar{l} = r\int_0^{2\pi} a_\varphi \, d\varphi = 0, \quad r > R \,. \tag{5.33}$$

This is illustrated in Figure 5.4.

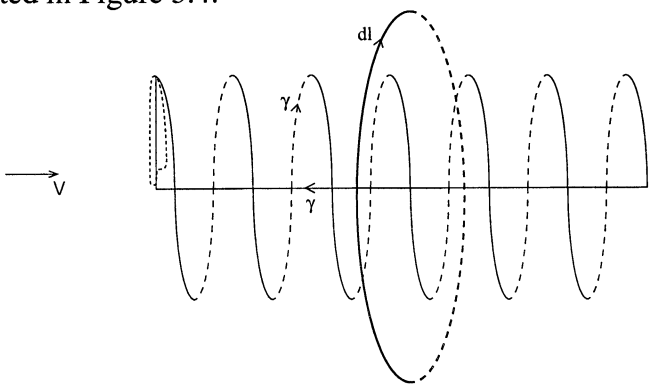

Figure 5.4
Integration curve in Ampère's circuital law.

When r < R, the integration curve encloses only the root vorticity, whose strength equals $-b\gamma$. Applying (5.31) gives

$$\oint \bar{a} \cdot d\bar{l} = r \int_0^{2\pi} a_\varphi d\varphi = -b\gamma, \quad r < R. \tag{5.34}$$

Combining (5.33) and (5.34) gives

$$\int_0^{2\pi} a_\varphi d\varphi = \begin{cases} -b\dfrac{\gamma}{r}, & 0 < r < R \\ 0, & R < r \end{cases}, \tag{5.35}$$

which is exactly (5.12).

5.4 The integrals of a_z^2 and $a_z a_\varphi$

For the integrals of a_z^2 and $a_z a_\varphi$, no explicit solutions were found. As was shown in Section 5.1, both C_{T_2} and C_{Q_2} are proportional to γ^2. For the dependence on d and R, no explicit relations were found.

The dependence on the number of blades is not as simple as one could hope. At $r = 0$, where the integrand does not depend on φ, we have, from equation (5.11), $a_z(r=0) = -b\gamma/d$ and hence

$$\int_0^{2\pi} a_z^2(0,\varphi) d\varphi = 2\pi \left(\frac{b\gamma}{d} \right)^2. \tag{5.36}$$

This means that the integrals of a_z^2 and $a_z a_\varphi$ are proportional to b^2 for small values of r, which also is verified numerically. However, for r close to the wake radius R and for r outside the wake, the integrals are found to be proportional to b.

5.5 Limit values when the pitch tends to infinity

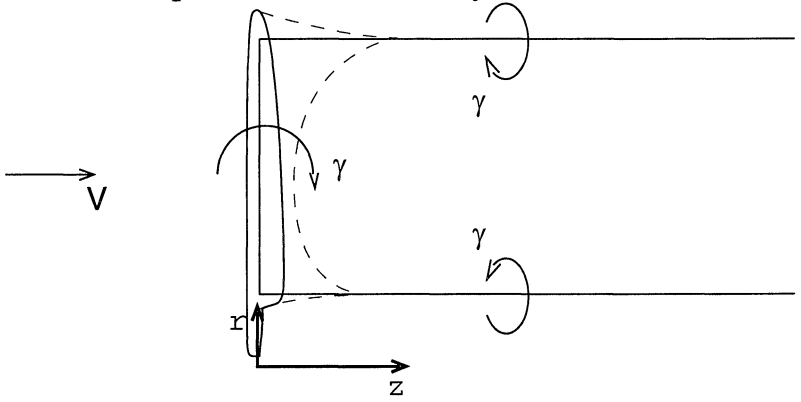

Figure 5.5
Parallel tip and root vortex, corresponding to a spiral with infinite pitch.

When $d \to \infty$, which corresponds for example to a non-rotating turbine, $a_z \to 0$ since there is no induced velocity parallel to a vortex line. Hence all integrals containing a factor of a_z tend to zero and so $C_T \to 0$ and $C_Q \to b\dfrac{\gamma}{\pi} R^2$ when $d \to \infty$.

5.6 Introduction of the function f

In the chapters above, the aerodynamic coefficients dependence on circulation is solved and some useful relations for radius and pitch are found. However, the dependence on pitch is not completely solved, nor the dependence on wake radius or number of blades. If a function ***f(b, d, R)*** is introduced, defined as

$$f(b,d,R) = \frac{d^2}{\pi\gamma^2} \int_0^{\infty} \int_0^{2\pi} a_z^2 d\varphi\, r dr \quad \left(= \frac{2d}{\gamma^2} \int_0^{\infty} \int_0^{2\pi} a_z a_\varphi d\varphi\, r^2 dr \right), \tag{5.37}$$

C_T and C_Q are given by

$$C_T = 2\frac{\gamma}{d}\left(bR^2 - \frac{\gamma}{d} \boldsymbol{f}(b, d, R) \right) \tag{5.38}$$

and

$$C_Q = \frac{\gamma}{\pi}\left(bR^2 - \frac{\gamma}{d} \boldsymbol{f}(b, d, R) \right) \tag{5.39}$$

respectively. (Compare to (3.20), (3.21), (5.13) and (5.14).) The only unknown variable in these equations is $\boldsymbol{f}(b, d, R)$, which is to be calculated numerically. It is notable that with this definition of $\boldsymbol{f}, \boldsymbol{f}$ does not depend on γ.

6 Inversion

So far the problem of calculating the thrust and torque coefficients from given spiral parameters has been treated, but the wanted result is a method to calculate the radius and pitch of the concentrated vortex spiral, from given values of C_T and C_Q and a given strength of the circulation.

Equation (5.5) gives an explicit and useful solution for the pitch, namely

$$d = 2\pi \frac{C_Q}{C_T}. \tag{6.1}$$

Calculating the wake radius is more complicated, since no explicit solution has been found. However, the aerodynamic coefficients' dependence on the circulation is solved and some useful relations are found. As is shown in the previous chapters, the formulas

$$C_T = 2\frac{\gamma}{d}\left(bR^2 - \frac{\gamma}{d} f(b,d,R)\right) \tag{5.38}$$

and

$$C_Q = \frac{\gamma}{\pi}\left(bR^2 - \frac{\gamma}{d} f(b,d,R)\right) \tag{5.39}$$

hold true, where the only unknown is $f(b, d, R)$.

The function $f(b, d, R)$ was calculated numerically for several values on radius and pitch. Since the dependence on the number of blades is not explicitly determined, new data base calculations are also needed for each value of the number of blades. Calculations were made for wind turbines and propellers with one to three blades. (For details, see Section 8.) This was accompliched by storing $f(b, d, R)$ in a database, but $f(b, d, R)$ is also shown in figures in Section 0.

The algorithm for calculating d and R from given values of C_T, C_Q, γ and b is as follows:

- Calculate d from (6.1).
- Use the calculated value of d to interpolate in the table of $f(b, d, R)$, in order to make a table of f as a function of only R.
- Use (5.38) and the table of $f(R)$ to make a table of C_T as a function of R only.
- Interpolate in this table to get R.

7 Root vortex model relations

In the main part of this work, the root vortex is modelled as a straight line along the wake centre axis. Another possibility is to model the root vortex as a small vortex spiral. The latter model does probably correspond better to the real case, but results in calculations that are more complex.

In this section, the size of the radius and pitch of the root vortex is discussed and some numerical examples are given.

7.1 Pitch and radius

The radius of the root vortex spiral depends on the shape of the blade. A typical value might be about 10% of the rotor radius.

The size of the pitch depends both on the velocities induced by the tip vortex and on self-induction. If t denotes the time for one revolution, the non-normalized tip vortex pitch is given by

$$d \cdot R_T = V\left(1+\frac{a_z}{2}\right)t \tag{7.1}$$

i.e. the mean value of the free stream velocity and the velocity inside the wake. If, for a first approximation, the self-induction is neglected, the non-normalized root vortex pitch is given by

$$d^*_{root} \cdot R_T = V(1+a_z)t\,. \tag{7.2}$$

This gives

$$d^*_{root} = d\frac{1+a_z}{1+\frac{a_z}{2}}\,. \tag{7.3}$$

Inserting the approximation $a_z \approx -b\frac{\gamma}{d}$ (compare with (5.11)) gives

$$d^*_{root} \approx d\frac{1-b\frac{\gamma}{d}}{1-b\frac{\gamma}{2d}}\,. \tag{7.4}$$

If the self-induction is taken into consideration, the non-normalized root vortex pitch is approximately given by

$$d_{root} R_T \approx V\left(1+a_z+\frac{a_{z\,root}}{2}\right)t\,, \tag{7.5}$$

where $a_{z\,root}$ has opposite sign compared to a_z. This gives

$$d_{root} \approx d\cdot\frac{1+a_z+\frac{a_{z\,root}}{2}}{1+\frac{a_z}{2}} \approx d\cdot\frac{1-b\frac{\gamma}{d}+b\frac{\gamma}{2d_{root}}}{1-b\frac{\gamma}{2d}}\,. \tag{7.6}$$

If d^*_{root}, calculated by (7.4), is inserted in the right hand side of (7.6), a rough approximation of d_{root} is obtained. Below follows a table of d_{root}, calculated for different tip vortex parameters. As can be seen, the difference between the tip and root vortex pitch is small, especially for large values of pitch.

γ	d	d^*_{root}	d_{root}
Propeller			
-0.5	0.7	0.88	0.74
-0.5	1	1.20	1.03
-0.5	5	5.24	5.01
-0.5	10	10.2	10.0
Turbine			
0.5	0.7	0.31	1.19
0.5	1	0.67	1.17
0.5	5	4.74	5.01
0.5	10	9.74	10.0

Table 7.1
Approximations of d_{root}, calculated for different values of tip vortex pitch. d^*_{root} denotes the first approximation of d_{root}, obtained by (7.4).

7.2 Explicit relations

Many of the relations found for the straight-line root vortex model can be applied to the spiral model, with only some small adjustments.

Modelling the root vortex as a spiral gives the relations

$$\int_0^{2\pi} a_z d\varphi = \begin{cases} -2\pi b\gamma\left(\dfrac{1}{d}-\dfrac{1}{d_{root}}\right), & 0<r<R_{root} \\ -2\pi b\dfrac{\gamma}{d}, & R_{root}<r<R \\ 0, & R<r \end{cases} \tag{7.7}$$

and

$$\int_0^{2\pi} a_\varphi d\varphi = \begin{cases} 0, & 0<r<R_{root} \\ -b\dfrac{\gamma}{r}, & R_{root}<r<R \\ 0, & R<r \end{cases} \tag{7.8}$$

which corresponds to (5.11) and (5.12) respectively and is shown in Figure 7.1 and 7.2 below. These formulas hold true for all values of the root vortex pitch. If $d_{root} \approx d$, (7.7) equals zero in the first interval. This corresponds to a wind velocity inside the root that equals the free stream wind velocity.

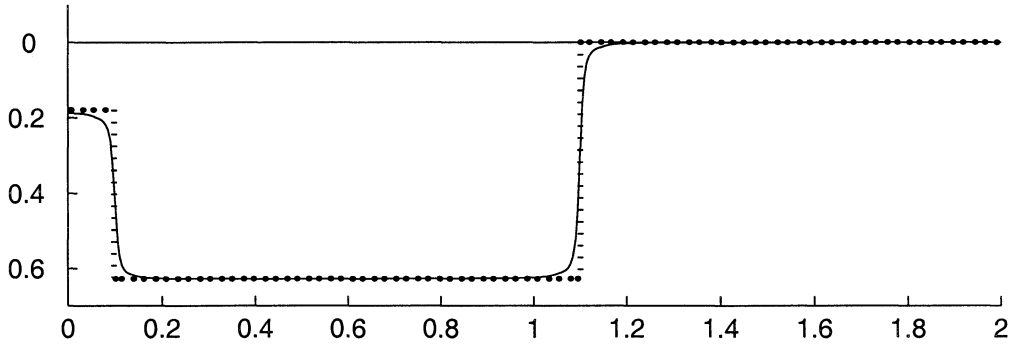

Figure 7.1
The result of a numerical integration of $a_z d\varphi$ (solid line), compared to (7.7) (dotted). (b = 1, R_{root} = 0.1, d_{root} = 7, R = 1.1, d = 5, γ = 0.5, R_{core} = 0.01.)

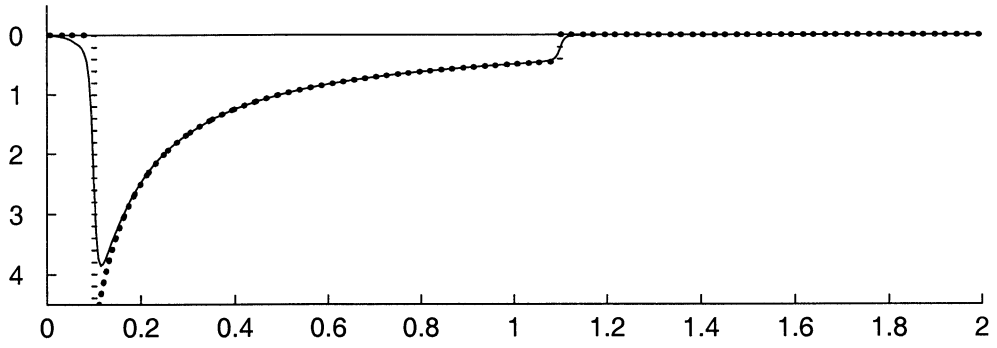

Figure 7.2
The result of a numerical integration of $a_\varphi d\varphi$ (solid line), compared to (7.8) (dotted). (b = 1, R_{root} = 0.1, d_{root} = 7, R = 1.1, d = 5, γ = 0.5, R_{core} = 0.01.)

Integrating in the r-direction gives

$$C_{T_1} = -\frac{2}{\pi}\int_0^{\infty}\int_0^{2\pi} a_z\, d\varphi\, r dr = 2b\gamma\left(\frac{R^2}{d} - \frac{R_{root}^2}{d_{root}}\right) \tag{7.9}$$

and

$$C_{Q_1} = -\frac{2}{\pi}\int_0^{\infty}\int_0^{2\pi} a_\varphi\, d\varphi\, r^2 dr = b\frac{\gamma}{\pi}\left(R^2 - R_{root}^2\right). \tag{7.10}$$

As in the case of the straight-line root vortex model, no explicit formula for calculating C_{T_2} and C_{Q_2} is obtained, but from the Biot-Savart law it follows directly that both are proportional to γ^2.

If the functions f_T and f_Q are introduced (compare (5.37) through (5.39)), C_T and C_Q can be expressed as

$$C_T = 2b\gamma\left(\frac{R^2}{d} - \frac{R_{root}^2}{d_{root}}\right) + \gamma^2 \cdot f_T\left(b, d, d_{root}, R, R_{root}\right) \tag{7.11}$$

and

$$C_Q = b\frac{\gamma}{\pi}\left(R^2 - R_{root}^2\right) + \gamma^2 \cdot f_Q\left(b, d, d_{root}, R, R_{root}\right) \tag{7.12}$$

respectively, where the functions f_T and f_Q can be calculated numerically.

If the root vortex pitch is of about the same size as the tip vortex pitch, i.e. if $d_{root} \approx d$, (5.5) is approximately true even if the root vortex is modelled as a spiral. That is,

$$\frac{C_T}{C_Q} \approx \frac{2\pi}{d}. \tag{7.13}$$

No database is made for this type of root vortex model, but some examples may show the differences between the methods.

7.3 Examples

Below follows a table of C_T and C_Q, calculated for the same values on the tip vortex parameters, but for different root vortex models. Both radius and pitch of the root vortex are varied.

As can be seen, the aerodynamic coefficients decrease for increasing root vortex spiral radius, but they do not change much when the root vortex pitch is varied. For small root vortex radii, the difference between the models is only a few percent.

R_{root}	d_{root}	C_T	C_Q
0	-	0.1581	0.1258
0.1	3	0.1527	0.1232
0.1	5	0.1554	0.1236
0.1	7	0.1564	0.1239
0.2	3	0.1384	0.1165
0.2	5	0.1478	0.1176
0.2	7	0.1516	0.1183

Table 7.2
C_T and C_Q calculated for different root vortex models.
$b = 1$, $R = 1.1$, $d = 5$, $\gamma = 0.5$.

8 Computer programming technicalities

8.1 Integration methods

The vortex spiral integral, giving the induced velocities in the Trefftz' plane, is divided into two parts. The first part, which is closest to the Trefftz' plane, is solved by numerical integration. The second part, which is far away from the Trefftz' plane, to be called the tail, is approximated by an analytically integrable function. That is

$$\int_0^\infty f(\theta)d\theta = \int_0^m f(\theta)d\theta + \int_m^\infty f(\theta)d\theta \approx \sum_{i=1}^{m/\Delta\theta} f(\theta_i)\Delta\theta + \int_m^\infty f_{approx}\,d\theta\,. \tag{8.1}$$

Integration of the flows in the Trefftz plane is performed by the Trapezoidal rule.

8.1.1 Numerical integration of the vortex spiral integral

The numerical integration of the vortex spiral integral is performed by approximating the integration curve by piecewise linear segments. To get the total induced velocity, at any chosen evaluation point in 3D space, the contributions of all line segments are added.

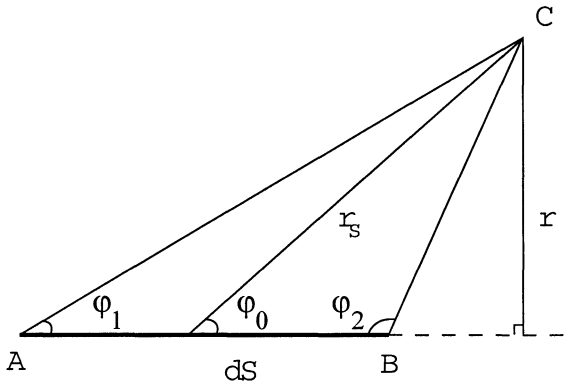

Figure 8.1
Vortex line A-B.

The velocity induced by a linear vortex line is perpendicular to the plane spanned by the vortex line and the evaluation point (that is, the plane *A-B-C* in Figure 8.1). According to Biot-Savart's law, (3.3), it is calculated as

$$\bar{a} = \frac{\gamma}{4\pi}\frac{\bar{r}_S \times d\bar{S}}{r_S^3} = \frac{\gamma}{4\pi}\frac{1}{r^2}\sin^3\varphi_0\, d\bar{S} \approx \frac{\gamma}{4\pi}\frac{r^2}{\left(r^2 + r_{core}^2\right)^2}\sin^3\varphi_0\, d\bar{S} \tag{8.2}$$

if dS is small compared to r or as

$$a = \frac{\gamma}{4\pi r}\left(\cos\varphi_1 + \cos\varphi_2\right) \approx \frac{\gamma}{4\pi}\frac{r}{r^2 + r_{core}^2}\left(\cos\varphi_1 + \cos\varphi_2\right) \tag{8.3}$$

otherwise. The right hand side formulas, applying the core approximation described in Section 3.3, are those used in the calculations. dS denotes the length of the vortex line element and r is the shortest distance between the evaluation point C and the (extended) vortex line. The vector $d\bar{S}$ defines the positive sense of γ, using the right hand screw rule. The angles φ_0, φ_1 and φ_2 are defined in Figure 8.1.

8.1.2 Tail approximation for the vortex spiral integral

Since numerical integration to infinity is impossible, an approximation of the integrand is made for large θ. The approximation is chosen such that it is analytically integrable and it is taken as the mean value of two functions, $f_{\max}$ and $f_{\min}$, bounding the integrand f. This gives

$$\int_m^{\infty} f_{\min}\,d\theta \le \int_m^{\infty} f d\theta \le \int_m^{\infty} f_{\max}\,d\theta \tag{8.4}$$

and

$$\int_m^{\infty} f d\theta \approx \frac{1}{2}\left(\int_m^{\infty} f_{\min}\,d\theta + \int_m^{\infty} f_{\max}\,d\theta\right). \tag{8.5}$$

The boundary functions used are, with some corrections, those presented by Chiu and Peters (1987).

Integrand approximation in the x-direction

$$f_x = \sum_{i=1}^{b} \frac{R\sin(\alpha_i-\theta)-r\sin(\varphi)+R\cos(\alpha_i-\theta)\theta}{\left(R^2+r^2-2rR\cos(\alpha_i-\theta-\varphi)+\left(\frac{d}{2\pi}\theta\right)^2\right)^{\frac{3}{2}}} \tag{8.6}$$

$$f_{x\,\min} = \sum_{i=1}^{b} \frac{R\sin(\alpha_i)-r\sin(\varphi)+R\cos(\alpha_i)\theta}{\left(R^2+r^2-2rR\cos(\alpha_i-\varphi)+\left(\frac{d}{2\pi}\theta\right)^2\right)^{\frac{3}{2}}} \tag{8.7}$$

$$f_{x\,\max} = \sum_{i=1}^{b} \frac{R\sin\left(\alpha_i+\frac{\pi}{b}\right)-r\sin(\varphi)+R\cos\left(\alpha_i+\frac{\pi}{b}\right)\theta}{\left(R^2+r^2-2rR\cos\left(\alpha_i+\frac{\pi}{b}-\varphi\right)+\left(\frac{d}{2\pi}\theta\right)^2\right)^{\frac{3}{2}}} \tag{8.8}$$

Integrand approximation in the y-direction

$$f_y = \sum_{i=1}^{b} \frac{-R\cos(\alpha_i-\theta)+r\cos(\varphi)+R\sin(\alpha_i-\theta)\theta}{\left(R^2+r^2-2rR\cos(\alpha_i-\theta-\varphi)+\left(\frac{d}{2\pi}\theta\right)^2\right)^{\frac{3}{2}}} \tag{8.9}$$

$$f_{y\,\min} = \sum_{i=1}^{b} \frac{-R\cos\left(\alpha_i+\frac{\pi}{2b}\right)+r\cos(\varphi)+R\sin\left(\alpha_i+\frac{\pi}{2b}\right)\theta}{\left(R^2+r^2-2rR\cos\left(\alpha_i+\frac{\pi}{2b}-\varphi\right)+\left(\frac{d}{2\pi}\theta\right)^2\right)^{\frac{3}{2}}} \tag{8.10}$$

$$f_{y\,\max} = \sum_{i=1}^{b} \frac{-R\cos\left(\alpha_i+\frac{3\pi}{2b}\right)+r\cos(\varphi)+R\sin\left(\alpha_i+\frac{3\pi}{2b}\right)\theta}{\left(R^2+r^2-2rR\cos\left(\alpha_i+\frac{3\pi}{2b}-\varphi\right)+\left(\frac{d}{2\pi}\theta\right)^2\right)^{\frac{3}{2}}} \tag{8.11}$$

Integrand approximation in the z-direction

$$f_z = \sum_{i=1}^{b} \frac{-R^2 + rR\cos(\alpha_i - \theta - \varphi)}{\left(R^2 + r^2 - 2rR\cos(\alpha_i - \theta - \varphi) + \left(\frac{d}{2\pi}\theta \right)^2 \right)^{\frac{3}{2}}} \tag{8.12}$$

$$f_{z\,\min} = \sum_{i=1}^{b} \frac{-R^2 + rR\cos(\alpha_i)}{\left(R^2 + r^2 - 2rR\cos(\alpha_i) + \left(\frac{d}{2\pi}\theta \right)^2 \right)^{\frac{3}{2}}} \tag{8.13}$$

$$f_{z\,\max} = \sum_{i=1}^{b} \frac{-R^2 + rR\cos\left(\alpha_i + \frac{\pi}{b}\right)}{\left(R^2 + r^2 - 2rR\cos\left(\alpha_i + \frac{\pi}{b}\right) + \left(\frac{d}{2\pi}\theta \right)^2 \right)^{\frac{3}{2}}} \tag{8.14}$$

8.1.3 Integration in the Trefftz plane

Integration in the Trefftz plane is, in both the radial and the angular direction, performed by the Trapezoidal rule. The Trapezoidal rule for integrating in the φ-direction is given by

$$\int_0^{2\pi} f(\varphi)d\varphi \approx \Delta\varphi\left(f(0) + f(\Delta\varphi) + f(2\Delta\varphi) + \ldots + f((n-1)\Delta\varphi)\right), \tag{8.15}$$

where $\Delta\varphi$ is the step size and $n = 2\pi/\Delta\varphi$ is the number of intervals.

The Trapezoidal rule for integration in the r-direction becomes

$$\int_a^b f(r)dr \approx \Delta r\left(\frac{f(a)}{2} + f(a+\Delta r) + f(a+2\Delta r) + \ldots + f(a+(n-1)\Delta r) + \frac{f(b)}{2} \right), \tag{8.16}$$

where Δr is the step size and the number of intervals is $n = (b-a)/\Delta r$. The step size Δr is not constant for all r. It is chosen smaller when r is close to a vortex line, since the curvature of the integrand is larger there.

8.1.4 Integration limits and step sizes

The step sizes and integration limits are a compromise between good accuracy and an acceptable calculation time. The step size in the vortex line integration is chosen as

$$\Delta\theta = \frac{2\pi}{360}. \tag{8.17}$$

This results, according to Bhagwat and Leishman (2001), in a relative error of about 10^{-3}.

The break point m, where the numerical integration in the θ -direction is substituted by the tail approximation is chosen as $m = 10\pi$. According to Chiu and Peters (1987), this results in a relative error of size 10^{-3}. Observe that the integration is not interrupted at $\theta = m$, there is only a change in integration method.

The integration of the flows in Trefftz' plane is made with the step sizes

$$\Delta\varphi = \frac{2\pi}{360} \tag{8.18}$$

and

$$\Delta r = \begin{cases} 0.5r_{core}, & |R-r| < 20r_{core} \text{ or } |R_{root}-r| < 20r_{core} \\ 0.1R, & r > 3R \\ 0.01R, & \text{otherwise} \end{cases} \tag{8.19}$$

In the radial direction, it is difficult to know when to interrupt the calculations. Since small deviations at large radii are multiplied by large areas, errors increase rapidly and the result depends to a great deal on when the calculation is interrupted. The break point where the integration is interrupted is chosen as $r = 10R$.

8.2 Calculation intervals

C_T and C_Q are given by (5.38) to (5.39), which are repeated below. The only unknown is the function $f(b, d, R)$, which is calculated numerically and stored in a database.

$$C_T = 2\frac{\gamma}{d}\left(bR^2 - \frac{\gamma}{d} f(b,d,R)\right) \tag{5.38}$$

and

$$C_Q = \frac{\gamma}{\pi}\left(bR^2 - \frac{\gamma}{d} f(b,d,R)\right) \tag{5.39}$$

The wake radius (R) is varied between 0.7 and 1.5, with the step size 0.1. Values less than 1.0 correspond to a propeller and values greater than 1.0 to a turbine. Values outside this interval correspond to an extreme increase or decrease in the wind speed and are quite unusual.

The relative pitch (d) can take all values between moderately negative and infinity, where negative values would correspond to the situation for a vertically descending helicopter. Calculations are limited to values between 0.1 and 25, with increasing step sizes as the pitch increases. The values for which calculations are made are

$$d = [0.1, 0.2, 0.4, 0.6, 0.8, 1.0, 1.5, 2, 2.5, 3, 3.5, 4, 5, 6, 7, 8, 9, 10, 12, 15, 18, 21, 25].$$

Calculations are only made for airscrews with one to three blades.

8.3 Interpolation

The input variables are C_T, C_Q and γ. The wake radius and pitch is calculated using the inversion algorithm described in Section 6.

A linear interpolation method is chosen for values inside the table. If an input value is outside the table, extrapolation is made by fitting a second-degree polynomial to the three endpoints in the table.

9 Program interface

Two different programs were made. One for calculating the function ***f(b, d, R)*** and making the database, called MakeDatabase, and one for interpolating in the database and calculating radius and pitch, called FindRD.

The program MakeDatabase is only needed if the database is to be extended, for example if one wants to study airscrews with more than three blades. In the main program, descriptions of how to change the parameter values are found.

The program FindRD is used for calculations of radius and pitch of the tip vortex spiral. When the program is run it asks, in the command window, for the values of b, C_T, C_Q and γ and returns the calculated values of R and d. A corresponding subroutine is also constructed, which can be included in a larger program.

10 The Function *f(b,d,R)*

In this section the calculated values of the function *f* is shown in figures. The increasing value on *f* for small pitch might look strange at a first glance, but corresponds to the situation when the induced velocity inside the wake is so large that the wind direction inside the wake is opposite to that of the free stream wind. This occures when the non-dimensional induced velocity is larger than one.

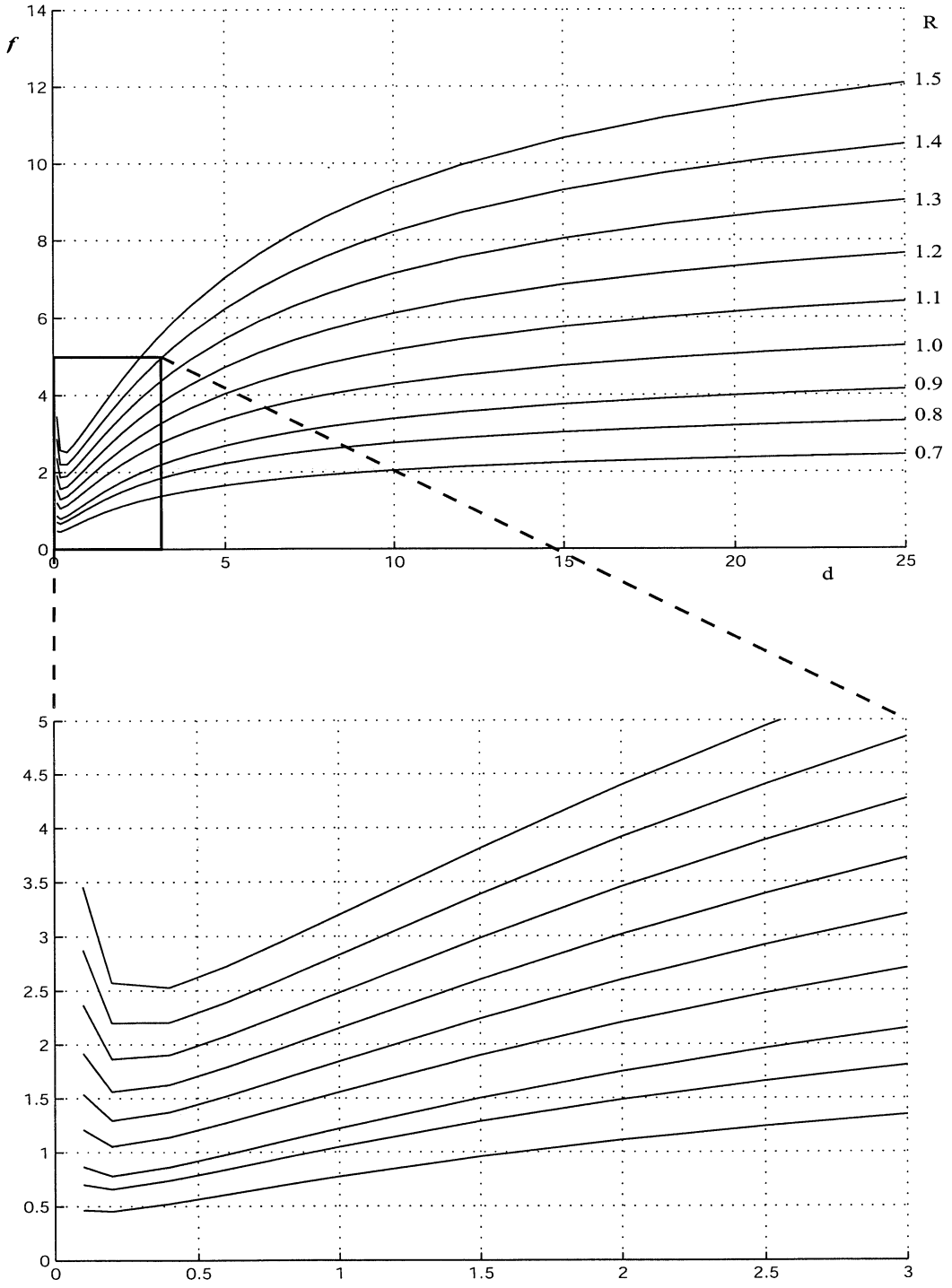

Figure 10.1

Wind turbine or propeller with one blade.
f as a function of pitch (d), plotted for different radii (R).

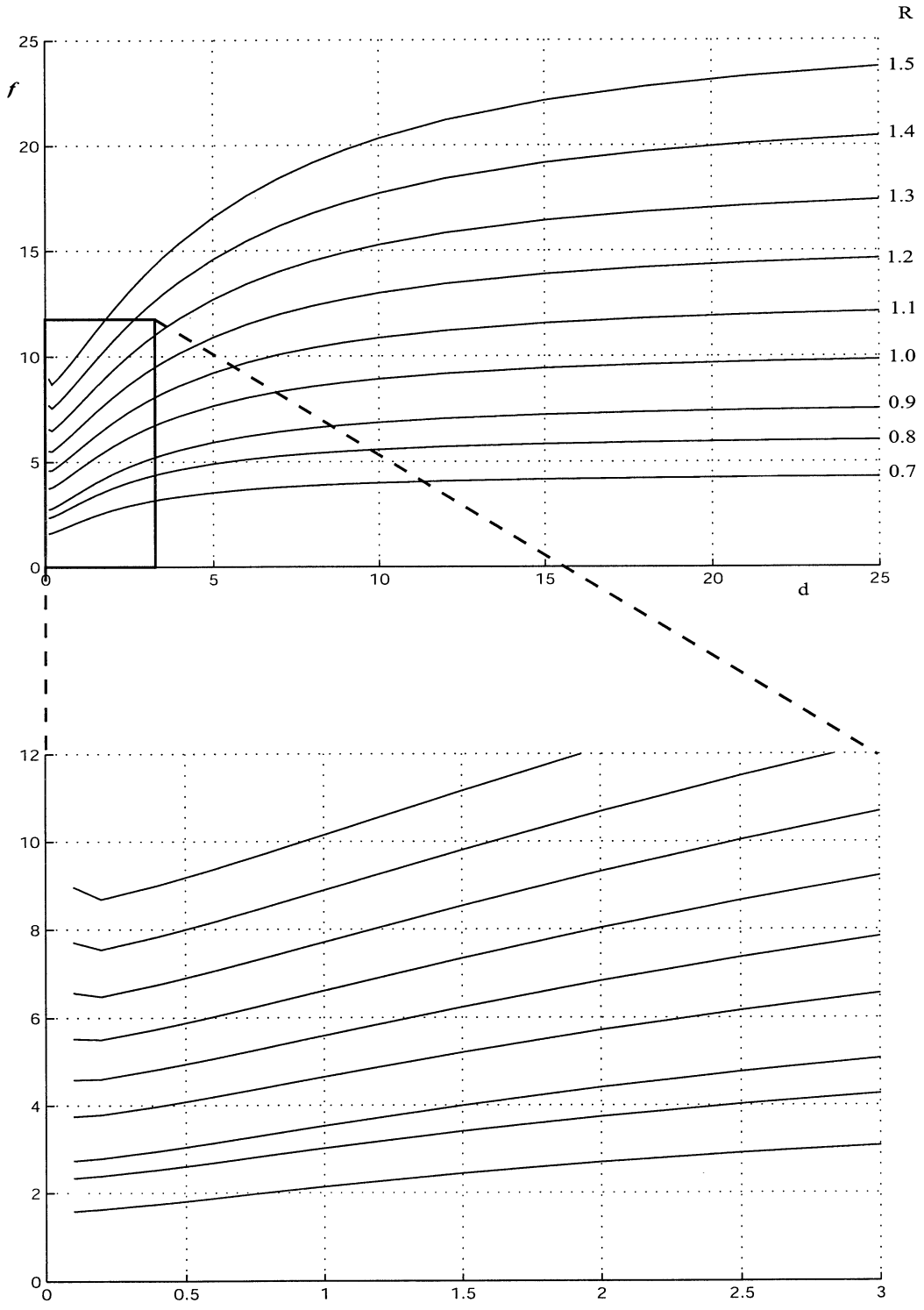

Figure 10.2
Wind turbine or propeller with two blades.
f as a function of pitch (d), plotted for different radii (R).

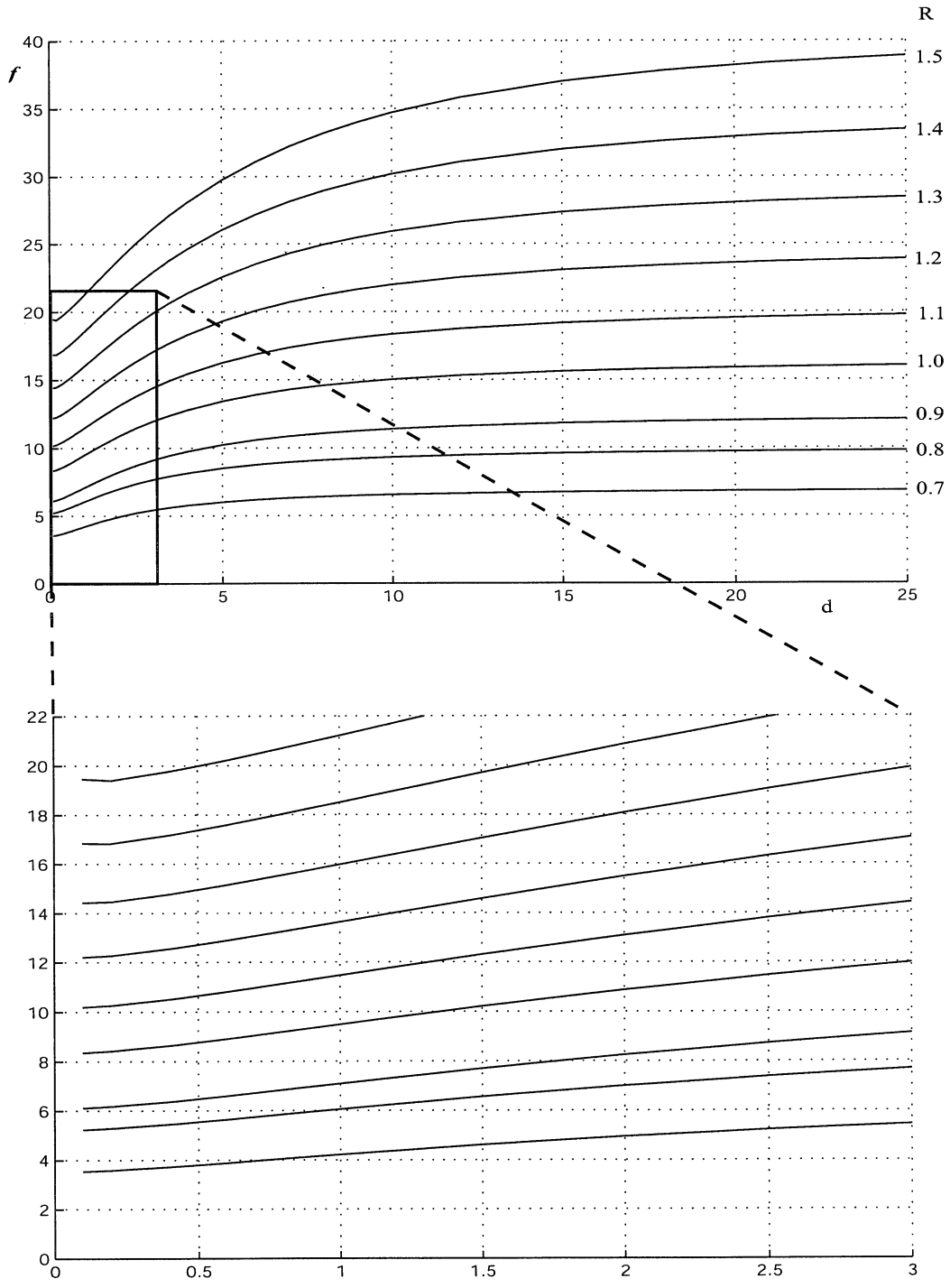

Figure 10.3
Wind turbine or propeller with three blades.
f as a function of pitch (d), plotted for different radii (R).

References

1. Ashley, H., & Landahl, M. (1965). *Aerodynamics of wings and bodies*. Reading, Massachusetts: Addison-Wesley Publishing Company.

2. Bhagwat, M. J., & Leishman, J. G. (2001). "Accuracy of straight-line segmentation applied to curvilinear vortex filaments". *Journal of the American Helicopter Society*, vol. 46, no. 2, pp. 166-169.

3. Cheng, D. K. (1989). *Field and wave electromagnetics*. Reading, Massachusetts: Addison-Wesley Publishing Company.

4. Chiu, Y. D., & Peters, D. A. (1987). "Numerical solutions of induced velocities by semi-infinite tip vortex lines". *Journal of Aircraft*, vol. 25, no. 8, pp. 684-694.

5. Eggleston, D. M., & Stoddard, F. S. (1987). *Wind turbine engineering design*. New York: Van Nostrand Reinhold Company.

6. Freris, L. L. (Ed.). (1990). *Wind energy conversion systems*. London: Prentice Hall.

7. Goldstein, S. (1929). "On the vortex theory of screw propellers". *Preceedings of the Royal Society of London*, series A, 123(1929), pp. 440-465. London: Royal Society of London.

8. Graber, A., & Rosen, A. (1987). "Velocities induced by semi-infinite helical vortex filaments". *Journal of Aircraft*, vol. 24, no. 5, pp. 289-290.

9. Hughes, W. F., & Brighton, J. A. (1967). *Fluid Dynamics*. New York: Schaum Publishing Company.

10. Lugt, H. J. (1983). *Vortex flow in nature and technology*. New York: John Wiley & Sons.

11. Rand, O., & Rosen, A. (1984). "Efficient methods for calculating the axial velocities induced along rotating blades by trailing helical vortices". *Journal of Aircraft*, vol. 21, no. 6, pp. 433-434.

12. Rosen, A., Lavie, I., & Seginer, A. (1990). "A general free-wake efficient analysis of horizontal-axis wind turbines". *Wind Engineerng*, vol. 14, no. 6, pp. 362-373. Essex, U.K.: Multi-Science Publishing Company.

13. Schlichting, H., & Truckenbrodt, E. (1960). *Aerodynamik des Flugzeuges*. Berlin: Springer-Verlag.

14. Schmidt, L. V. (1998). *Introduction to aircraft flight dynamics*. Reston, Virginia: American Institute of Aeronautics and Astronautics.

15. Spera, D. A. (Ed.). (1994). *Wind turbine technology. Fundamental concepts of wind turbine engineering*. New York: Asme Press.

16. Theodorsen, T. (1948). *Theory of propellers*. New York: McGraw-Hill Book Company.

17. Von Mises, R. (1945). *Theory of flight*. New York: McGraw-Hill Book Company.